NANO LETTERS

Letter

Cite This: Nano Lett. 2017, 17, 6557-6563

pubs.acs.org/NanoLett

Perovskite Nanowire Extrusion

Sebastian Z. Oener,[†,‡] Parisa Khoram,[†] Sarah Brittman,[†] Sander A. Mann,[†] Qianpeng Zhang,[§] Zhiyong Fan,[§] Shannon W. Boettcher,[‡] and Erik C. Garnett*[,†]

[†]Center for Nanophotonics, AMOLF, Science Park 104, 1098 XG Amsterdam, The Netherlands

[‡]Department of Chemistry and Biochemistry, University of Oregon, Eugene, Oregon 97403, United States

[§]Department of Electronic and Computer Engineering, The Hong Kong University of Science and Technology, Clear Water Bay, Kowloon, Hong Kong SAR, China

Supporting Information

ABSTRACT: The defect tolerance of halide perovskite materials has led to efficient optoelectronic devices based on thin-film geometries with unprecedented speed. Moreover, it has motivated research on perovskite nanowires because surface recombination continues to be a major obstacle in realizing efficient nanowire devices. Recently, ordered vertical arrays of perovskite nanowires have been realized, which can benefit from nanophotonic design strategies allowing precise control over light propagation, absorption, and emission. An anodized aluminum oxide template is used to confine the crystallization process, either in the solution or in the vapor phase. This approach, however, results in an unavoidable drawback: only nanowires embedded inside the AAO are obtainable, since the AAO cannot be etched selectively. The requirement for a support matrix originates from the intrinsic difficulty of controlling precise placement, sizes, and shapes of free-standing nanostructures during crystallization, especially in solution. Here we introduce a method to fabricate free-standing solution-based vertical nanowires with arbitrary dimensions. Our scheme also utilizes AAO; however, in contrast to embedding the perovskite inside the matrix, we apply a pressure gradient to extrude the solution from the free-standing templates. The exit profile of the template is subsequently translated into the final semiconductor geometry. The free-standing nanowires are single crystalline and show a PLQY up to ~29%. In principle, this rapid method is not limited to nanowires but can be extended to uniform and ordered high PLQY single crystalline perovskite nanostructures of different shapes and sizes by fabricating additional masking layers or using specifically shaped nanopore endings.

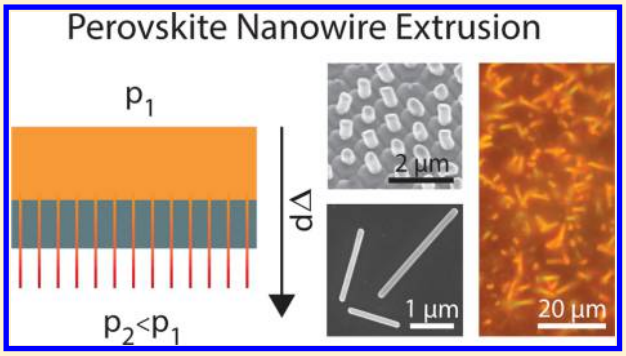

KEYWORDS: *Perovskite, nanowires, array, solution, extrusion, AAO*

Solution-based halide perovskite materials have attracted tremendous attention over the last five years. Their remarkable tolerance to defects has allowed for the rapid fabrication of structures with a high photoluminescence quantum yield directly from solution. They show great potential for optoelectronic devices, most prominently solar cells and light-emitting diodes.[1,2] While most research efforts have focused on thin-film geometries, highly ordered nanostructure array geometries have attracted less attention, even though nanophotonic design strategies allow precise control over light propagation, absorption, and emission.[3−11] For example, while several reports exist on the formation of perovskite nanowires,[12−28] only a few of them show highly ordered vertical array geometries, which are of prime importance for solar cell and LED applications.[25−28]

Only recently, ordered vertical perovskite nanowire arrays inside anodized aluminum oxide (AAO) templates have been realized.[25−28] In these studies, the AAO confines the crystallization process in either solution or vapor phase and therefore completely determines the cross-section and length of the final nanostructures. Since the AAO cannot be removed selectively, because of the sensitivity of perovskites to etchants, the nanowires remain embedded inside the AAO and are not free-standing arrays. Also, the geometries achievable with this approach are limited to what can be obtained in AAO.

In general, synthetic methods for making free-standing solution-based nanostructure arrays with arbitrary cross-sectional shapes and sizes are currently lacking. This limitation can be explained by the intrinsic difficulty of controlling the precise placement and form factors of free-standing nanostructures during crystallization from solution.

Here we introduce a method to fabricate nanostructure arrays with arbitrary dimensions directly from solution. As proof of this concept, we show the fabrication of vertical free-standing $CH_3NH_3PbBr_3$ perovskite nanowires. The scheme utilizes AAO templates to confine the precursor solution in

Received: May 25, 2017
Revised: September 19, 2017
Published: October 2, 2017

DOI: 10.1021/acs.nanolett.7b02213
Nano Lett. 2017, 17, 6557−6563

highly ordered nanopores with narrow size distributions. In contrast to techniques that embed the perovskite inside the AAO, the solution is extruded from the free-standing templates, driven by a small pressure gradient of 50−100 mbar versus atm. At this stage the formation of the nanowire-shaped intermediate crystal phase is initiated by more rapid evaporation of the solvent near the pore exits and the confinement of the solution. The pore exits therefore determine the dimensions of the nanostructures. After annealing, highly uniform free-standing perovskite nanowires with a wide variety of dimensions are obtained. Transmission electron microscopy (TEM) diffraction shows single crystallinity along the length of the nanowire. Photoluminescence quantum yield (PLQY) measurements on single nanowires reach values of ∼29%, which are in line with values for $CH_3NH_3PbBr_3$ thin films.[29−31]

In principle, this novel method is not limited to nanowire arrays but could be extended to a large variety of highly uniform and ordered high PLQY single crystalline perovskite nanostructures. Different shapes and sizes could be obtained by fabricating additional masking layers or using specifically shaped nanopore endings.[32] The concept of the fabrication process is very similar to macroscopic profile extrusion in the plastics industry, however, for a nanoscale optoelectronic material. The unprecedented simplicity and high speed make it therefore a highly promising approach for the industrial fabrication of novel optoelectronic devices based on high PLQY nanostructured arrays.

Figure 1 shows the fabrication scheme. In the first step (Figure 1a), the $CH_3NH_3PbBr_3$ solution (3 M in dimethyl sulfoxide, DMSO) is dropcast onto a free-standing AAO template (30−50 μm thick), which rests on an O-ring on top of a PDMS block. AAO is a well-known template for nanostructuring and allows control over pore size and shape from hundreds of nanometers down to around 5 nm on a wafer scale and even in binary array geometries.[32−37] By selectively etching the supporting aluminum substrate, free-standing AAO templates with double-sided pore access can be obtained.[38,39] To facilitate the filling of the AAO pores with the perovskite solution, a low-pressure region is formed in the sealed air compartment between the AAO and the PDMS. We use a simple syringe connected via a plastic tube to establish the pressure gradient of 50−100 mbar versus atm when pulling the piston of the syringe. In general, any method to control the pressure can be utilized. Driven by the pressure gradient across the membrane, the perovskite solution rapidly fills the AAO pores and extrudes out of the AAO template on the bottom (inset in Figure 1a). The whole extrusion takes only ∼30 s (see Methods).

By breaking off the nanowires and transferring them to a different substrate, we show that an intermediate crystal phase probably consisting of $CH_3NH_3PbBr_3$ including coordinated DMSO molecules is formed in the nanowire shape right at this stage, that is, before the subsequent annealing (see SI). Such intermediates have been reported previously.[40−43] The crystallization of the intermediate is likely due to preferential evaporation of the solvent from the pore exit and the solution confinement inside the AAO pores. In the next step, the template is carefully transferred onto glass spacers positioned on a hot plate and annealed at 120 °C to form the perovskite crystals (Figure 1b). The required annealing time varies from about 10−90 min, depending on the amount of residual perovskite solution on the top surface of the template. Figure 1c shows schematically the final AAO template with the extruded free-standing nanowires. The diameter of our AAO templates spans about 4−10 mm, but free-standing templates with diameters of up to 100 mm are available commercially. Finally, we dry-transfer the perovskite nanowires to different substrates (glass, silicon, TEM grids) for subsequent characterization. We have used the same AAO templates numerous times, simply by dissolving the residual perovskite inside the pores with DMSO and rinsing in acetone and isopropanol followed by prolonged annealing. Therefore, the requirements for a reusable substrate scheme, for example, by embedding the array of nanostructures into a polymer layer followed by mechanical peel-off, are easily met.

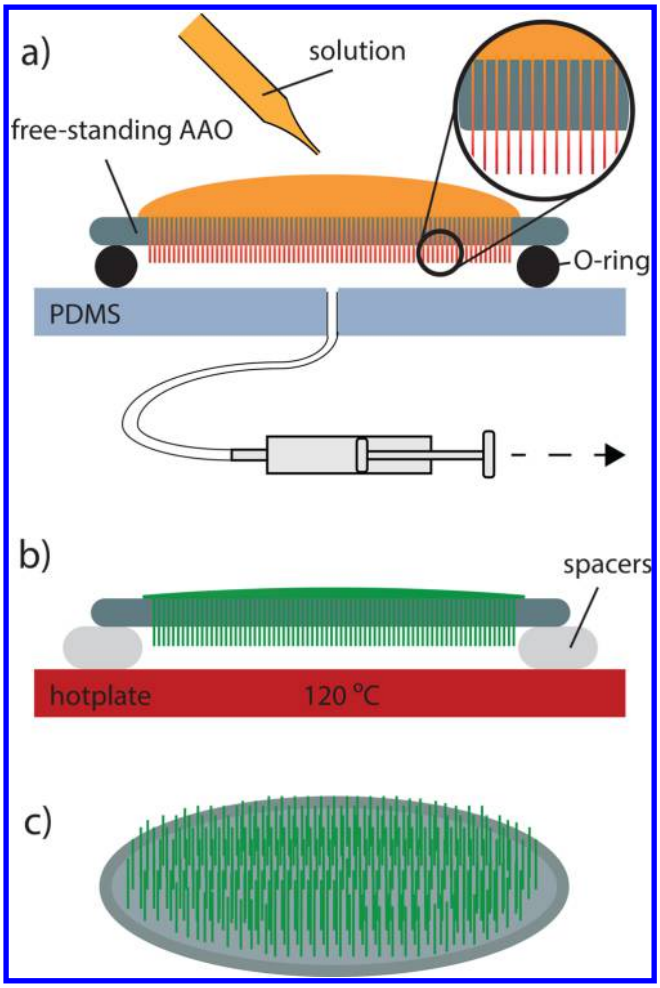

Figure 1. Perovskite nanowire extrusion scheme: (a) $CH_3NH_3PbBr_3$ solution (3 M in DMSO) is dropcast onto an AAO template placed on an O-ring on top of a PDMS block. A low pressure region is formed in the sealed air compartment between the AAO and the PDMS block with a glass syringe connected via plastic tubing. After a short time (∼30 s) the perovskite solution fills the AAO pores and extrudes out of the AAO template on the bottom (inset). (b) The template is carefully transferred to a hot stage and annealed. (c) The final AAO template with extruded free-standing nanowire arrays.

Figure 2a shows extruded free-standing vertical perovskite nanowires covering a wide area of the AAO surface (∼1 cm^2). The length of the nanowires is dictated directly by the time the pressure gradient is applied to the template. As shown in Figure 2a longer nanowire arrays are realized when applying the pressure gradient for a longer time. While our current results serve as as proof of concept, further optimization is necessary to

DOI: 10.1021/acs.nanolett.7b02213
Nano Lett. 2017, 17, 6557−6563

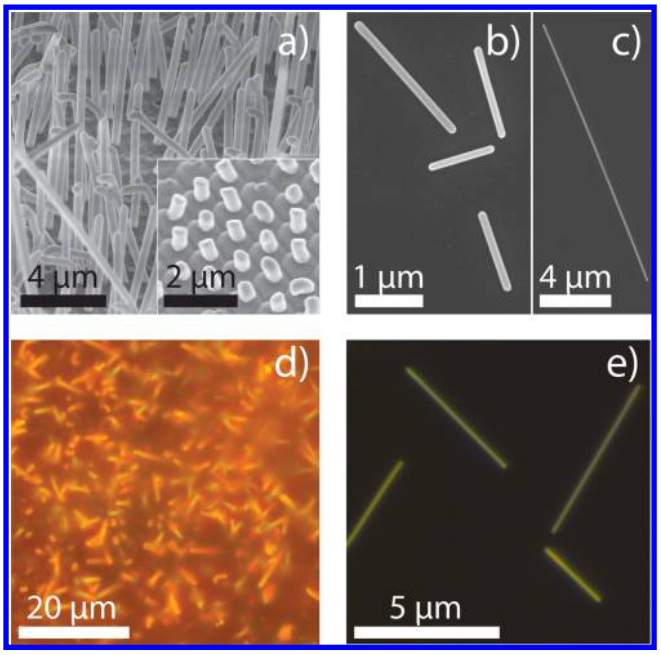

Figure 2. Electron and optical microscopy images of extruded perovskite nanowires: (a) SEM image of vertical nanowires. Inset shows shorter nanowires that have been obtained by exposing the template for shorter times to the pressure gradient. (b, c) Higher magnification SEM images of single horizontal perovskite nanowires with different wire lengths. (d) Optical top view dark-field microscope image of a random array under white light illumination. (e) Optical dark-field microscope image of single nanowires.

improve the wire-to-pore ratio, diameter distribution and nanowire length. In this study, two different types of AAO templates were used: commercially available semiordered templates with average pore sizes of 200 nm (pitch 470 nm) and custom-made ordered templates with pore size of 250 nm (pitch 1 μm) (Figure 2). The pitch-to-pore ratio serves as a crucial parameter in realizing nanowire arrays; for ratios smaller than ~4 the extruded nanowires coalesce (see SI). To increase the initial ratio, the pore sizes of the semiordered templates were shrunk down by subsequent atomic layer deposition of alumina (see Methods and Figure SI3). As indicated in Figure 2b, the average nanowire diameter employing the final template was ~160 nm. We observed an increase in diameter compared to the AAO pore exit (~120 nm), which we attribute to a nonideal contact angle between the pore wall and the back surface of the template, which leads to partial surface wetting around the pore instead of immediate extrusion. With increasing time of mechanical polishing to obtain a 90° angle, we observed a decreasing discrepancy between pore exit and the final nanowire diameter. The thin wires were used for TEM studies, while the thick nanowires fabricated from ordered AAO templates were used for PLQY measurements, as described further. Figure 2c shows a nanowire with a length of ~20 μm, originating from a template which was exposed for a longer time to the pressure gradient (details in Methods). The SEM images demonstrate high geometric uniformity and absence of any apparent surface disorder on the nanowires. Figure 2d shows an optical dark-field image taken from a vertical nanowire array illuminated with white light from the top. In Figure 2e an optical dark-field image of single nanowires is shown, which supports the high uniformity of the wires by the absence of strong optical variations along the length or in between nanowires, for example, due to changing optical resonances because of variations in diameter.[44,45]

To obtain crystallographic information, we performed transmission electron microscopy (TEM) diffraction on single perovskite nanowires and X-ray diffraction (XRD) measurements on a whole template. Figure 3a shows a bright-field

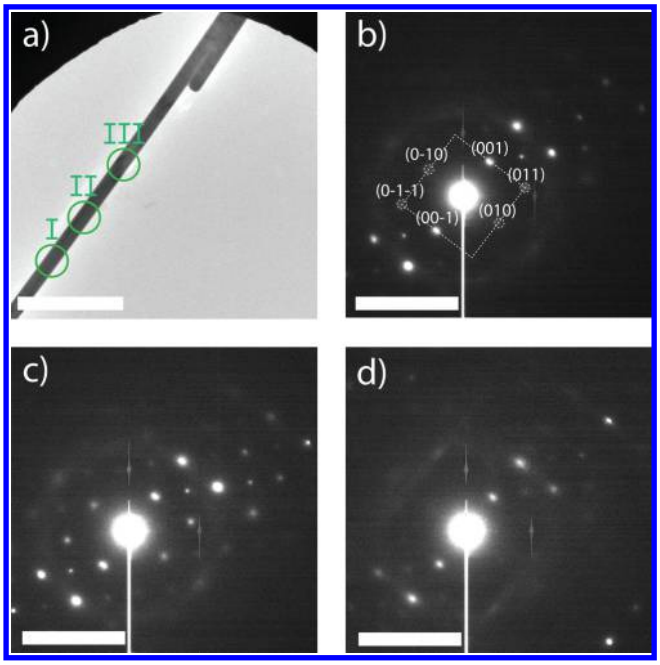

Figure 3. TEM single wire diffraction: (a) Bright-field image of a single perovskite nanowire. (b–d) Diffraction images of the regions I–III marked in panel a, respectively. The same diffraction spot pattern can be clearly seen along the length of the wire, confirming a single crystal phase. The obtained lattice constant for the wire, a = 5.85(5) Å, is in agreement with the literature value of $CH_3NH_3PbBr_3$ perovskite (a = 5.92 Å).[46] The scale bars in a and b–d are 2 μm and 2 nm^{-1}, respectively.

image of a wire with the green marked regions (I, II, III) indicating the locations of selected-area diffraction measurements, as shown in Figure 3b-3d, respectively (another wire is shown in the SI). The same diffraction spot pattern can be clearly seen along the length of the wire, confirming it is a single crystal. Furthermore, all of the measured wires via TEM diffraction showed a ⟨100⟩ growth direction for the cubic symmetry. The obtained lattice constant of a = 5.85(5)Å is in agreement with previously reported values for $CH_3NH_3PbBr_3$ perovskite (a = 5.92 Å).[46,47] Besides the 0.5–1% difference between the measured and the literature value of the lattice constant, we observe a set of symmetric diffraction spots not originating from the perfect cubic lattice, but which can be explained by a slight tilt of the octahedra in the crystal structure.[48,49] Therefore, we attribute the difference in lattice constants to a deviation from the perfect cubic crystal phase.[49] During electron beam exposure we observed degradation of the perovskite crystal, as already noted by others.[50] The exposure resulted in a continuous conversion to polycrystallinity, that is, the evolution of diffraction rings from distinct spot patterns with increasing exposure time which prevented perfect alignment to the zone axis (more details in the SI). The XRD measurements (see SI) confirm the dominance of the ⟨100⟩ growth direction over the whole template. When XRD is conducted on assembles of nanowires with a ⟨100⟩ growth

DOI: 10.1021/acs.nanolett.7b02213
Nano Lett. 2017, 17, 6557–6563

direction, the (100) and (200) crystal planes are expected to show the strongest diffraction peaks. These results prove that highly uniform and single crystalline perovskite nanowires can be obtained with this novel nanowire extrusion method.

To study the electronic and optical properties we performed photoluminescence quantum yield (PLQY) measurements (Figure 4). The PL spectrum in Figure 4a shows a peak centered at 535 nm, which is in agreement with previous reports for thin films of $CH_3NH_3PbBr_3$.[51] To obtain spatially resolved PLQY measurements of single nanowires, we used integrating sphere microscopy.[52,53] This technique allows us to determine quantitatively the spatially resolved absorptance, by using an integrating sphere to measure all nonabsorbed light and a glass sample holder on a piezo-stage to scan the sample across the laser beam. Additionally, by placing filters in front of the integrating sphere and reflection photodetectors, we can measure the photoluminescence quantitatively, as well.[42] As a result, we can calculate the spatially resolved PLQY, that is, how many photons are emitted per absorbed photon (see Methods). As can be seen in Figure 4b, the PLQY has the highest value of 29.5% at the center of the nanowire, while the average along the whole length is ∼20%. TEM measurements in Figure 3 confirm the single-crystalline nature of these wires, while the PLQY shows deviations of ±5% (abs.) from the average value along the nanowire length (Figure 4b). Given that the single-crystalline wire has no grain boundaries, we suspect surface recombination and defect recombination from slight variations in stoichiometry or point defect density to be the main factors limiting the performance.[30] It has been reported in previous studies that inhomogeneous vacancy distributions in perovskite single crystals lead to inhomogeneous PL.[54] We note that integrating sphere microscopy on single nanowires presents an ideal tool to study the influence of novel surface treatments and compositional variations on the electronic and optical performance of nanowires, because it excludes inhomogeneity at the array level.[55−57]

To study the degradation behavior of the nanowires in ambient conditions, we measured the PLQY over a period of 10 days (Figure 4c). The average PLQY decays from ∼20% to ∼5% (PLQY maps over a 10 day period are shown in the SI).

The PLQY of the nanowire as a function of incident laser intensity (see SI) shows a linear dependence with laser intensity (between 100 and 1000 suns), which can be explained by the Shockley−Read−Hall (SRH) recombination as the main limiting mechanism (rather than radiative or Auger recombination).[53] Therefore, we can extrapolate the PLQY down to 1 sun, which results in a value of ∼1% for the measured wire, comparable to reported values of 3% for $CH_3NH_3PbBr_3$ thin films with a 1:1 ratio ($MABr:PbBr_2$).[30] We have observed lower PLQY values for nanowires extruded from freshly prepared solutions, while the higher values shown here come from extrusion of aged solutions. Such a variation suggests that the nanowire extrusion process has the same strong dependence on the exact preparation conditions of the precursor solution as has been observed in thin films. Thin-film studies have concluded that preparation details including aging[58] and temperature[59] of the solution, solvent, and precursors,[60] precursor ratio,[47] and ambient conditions[61,62] all strongly influence the resulting material properties.

In conclusion, solution-based nanostructure extrusion enables the fabrication of free-standing perovskite nanowire arrays. Our crystallographic and optical measurements show single crystallinity along the lengths of the nanowires and

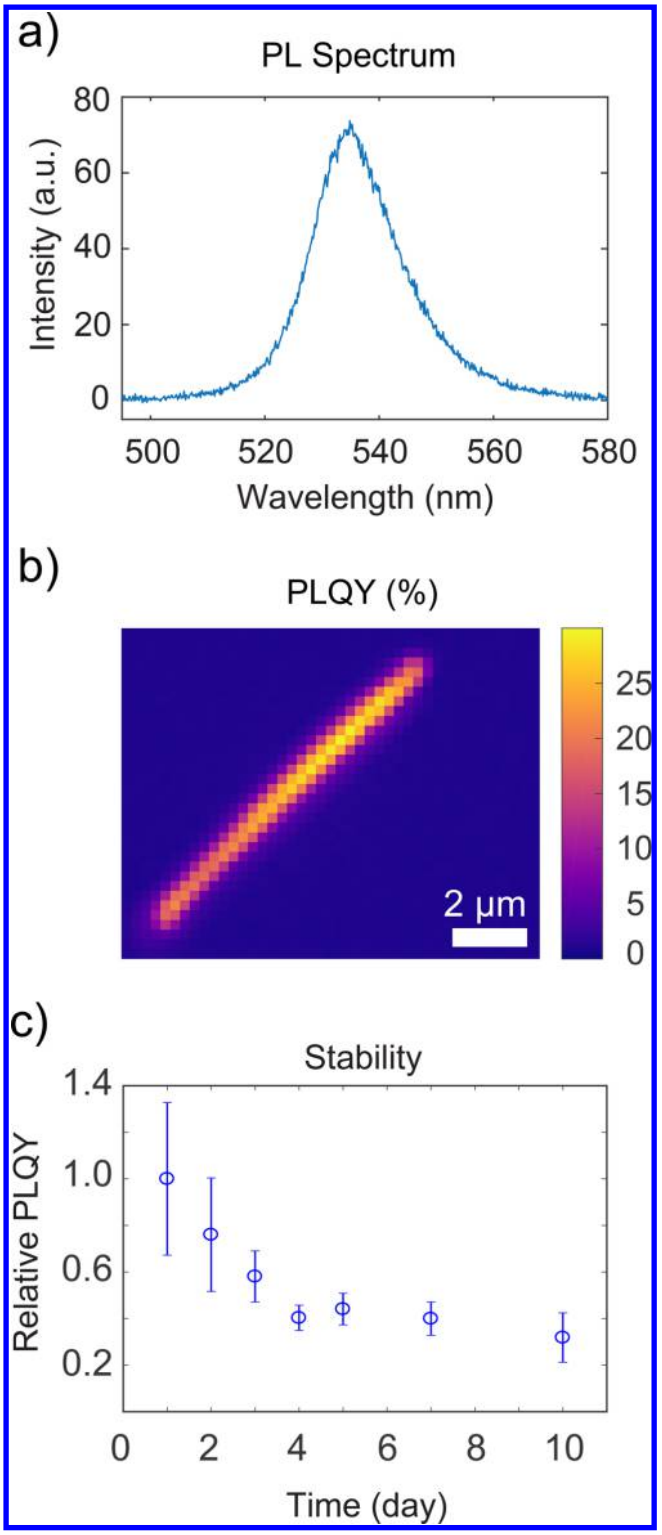

Figure 4. PLQY measurements of a single perovskite nanowire: (a) Nanowire photoluminescence (PL) spectrum at the center of the nanowire with a peak centered at 535 nm. (b) PLQY map at 1000 suns illumination intensity. (c) Mean relative PLQY with respect to day 1. After 10 days the PLQY decays by ∼70% from its initial value. The error bars are the standard deviation of the PLQY values along the nanowire.

PLQY values of up to 29%. This novel method can be generalized from nanowire arrays to other nanostructured shapes by altering the extrusion mask. Furthermore, provided

DOI: 10.1021/acs.nanolett.7b02213
Nano Lett. 2017, 17, 6557−6563

the stability issues for perovskite based systems are resolved, for example, by embedding the material in a flexible polymer encapsulation, the application extends potentially beyond research. The unprecedented simplicity and high speed of this novel nanostructure extrusion technique might be suitable for the industrial fabrication of nanostructured optoelectronic devices.

Methods. *Preparation of Methylammonium Lead Bromide ($CH_3NH_3PbBr_3$).* The solution was prepared at room temperature and in ambient conditions. CH_3NH_3Br was synthesized and recrystallized using a previously reported protocol.[63] The precursor $PbBr_2$ (Sigma-Aldrich, purity ≥98%) was mixed with CH_3NH_3Br in a 1:1 molar ratio with DMSO (Sigma-Aldrich, anhydrous, purity ≥99.5%) to obtain the 3 M solution. The fresh solutions were heated up to 60 °C and stirred with a magnetic stirrer for 1 1/2 h. The solution could be used for the extrusion right away resulting in nanowires with PLQY < 5% but was typically aged for 10−20 days at ambient conditions to allow for PLQY values of up to ∼30%. Prior to use the solution was heated to 70 °C while stirring.

Preparation of AAO Templates. Two types of AAO templates were used in this study. The commercially available free-standing AAO templates were purchased from InRedox with a pore size of 200 nm and a pitch of 470 nm. Atomic layer deposition of 50 nm Al_2O_3 was performed on these templates to narrow down the pore diameter to about 100 nm. This way, the spacing between two neighboring pores increased to avoid coalescence of individual nanowires into bundles. The final nanowire diameter is strongly influenced by the shape of the pore exit. Therefore, we mechanically polished the templates with polishing paper (4000, 6000, and 8000 grit) followed by a 10s HF (1%) etch and rinse in deionized H_2O to remove residual Al_2O_3 clogging the pores, with the side effect of slightly increasing the average pore diameter by about 20 nm. After the H_2O rinse, the templates were annealed for 2−3 h at 250 °C in air on clean glass slides. The final AAO templates had pore sizes of about 120 nm and provided nanowires with diameters of about 160 nm. This process unavoidably clogs some of the pores. Therefore, custom-made ordered AAO templates were prepared. Specifically, Al foil was cut into 1.5 cm × 2.5 cm pieces and cleaned in acetone, isopropyl alcohol, and deionized water with sonication, respectively. The foils were then electrochemically polished in a 1:3 mixture of perchloric acid and ethanol for 150 s at 12.5 V and 10 °C. The polished Al foils were then imprinted by 5 mm × 5 mm homemade silicon master (hexagonally ordered pillar array with height of 200 nm and pitches of 866 and 1000 nm) with a pressure of $\sim 2 \times 10^4$ N cm^{-2} to initiate the perfectly ordered AAO growth. Thereafter, Al chips were anodized with a home-built anodization setup with a voltage equal to pitch (nm)/ 2.5, and the anodization solution was made by mixture of 4 wt % citric acid, ethylene glycol, and 0.1 wt % sulfuric acid with a ratio of 115:115:10 (v/v/v). The anodization was continued for 36 h to give an AAO thickness of ∼40 μm. After that the AAO film was delaminated from the remaining aluminum by immersing the sample in over saturated $HgCl_2$. After aluminum was completed etched away, the sample was rinsed by acetone and then baked at 80 °C. Then the bottom side of the freestanding AAO film was opened by ion milling with 85° tilted angle at 750 V for 2 h.

Pressure Gradient and Nanowire Extrusion. To facilitate the filling and extrusion of the AAO pores by the perovskite solution, a pressure gradient of 50−100 mbar was applied across a 1 cm^2 AAO template, using an O-ring, a PDMS block, and a syringe. A 5 mL syringe was connected via a plastic tube and hole in the PDMS block. Then the solution was dropcast onto the AAO top surface, and the syringe was slowly pulled outward at a rate of about 0.5 mL/s to maintain a pressure gradient. The extrusion took about 30 s. While this procedure is suitable for a simple lab setup, a more controlled environment can be easily created with standard vacuum techniques. Due to the pressure gradient with the ambient, the perovskite solution slowly fills the whole AAO template until it reaches the AAO pore exit on the back.

Subsequently, the templates were carefully transferred to glass spacers on a hot stage and annealed at 120 °C for 10−90 min, depending on the amount of residual perovskite solution on the AAO top surface. We note that the perovskite crystal structure is rapidly formed during the first few minutes of annealing, due to the evaporation of DMSO from the nanowire intermediate, and most of the annealing time is required to remove enough solvent from the template to avoid complication during the subsequent handling. To transfer the nanowires to different substrates (glass, silicon, TEM grid) for subsequent characterization, the wires were broken off by sliding the respective substrate over the AAO template.

TEM Diffraction. The TEM diffraction measurements were done on a 300 keV TEM (FEI 80-300 Titan) at the Center for Advanced Materials Characterization in Oregon (CAMCOR). The selected-area diffraction aperture was 40 μm. A Au TEM grid was used to avoid chemical reactions of the perovskite nanowires with the grid.

PLQY Measurements. The PLQY was measured in a home-built integrating sphere microscopy setup, employing a Fianium WL-SC-390-3 supercontinuum laser combined with an acousto-optic tunable filter (Crystal Technologies) to excite the sample at a wavelength of 480 nm. To distinguish between absorption and photoluminescence, we used short- and long pass filters with a cut off wavelength of 500 nm (Thorlabs FELH500 and FESH500). PLQY maps were obtained by dividing the map of emitted photons by the maximum number of absorbed photons. Average PLQY values were calculated from the PLQYs along the nanwire axis, and error bars are one standard deviation from the mean.

Further details of the integrating sphere microscopy technique have been reported previously.[52,53]

■ ASSOCIATED CONTENT

Supporting Information

The Supporting Information is available free of charge on the ACS Publications website at DOI: 10.1021/acs.nanolett.7b02213.

Wire-like intermediate crystal phase, TEM diffraction of additional perovskite nanowire, electron beam-induced damage during TEM studies (PDF)

■ AUTHOR INFORMATION

Corresponding Author

*E-mail: garnett@amolf.nl.

ORCID

Sebastian Z. Oener: 0000-0003-0770-4089
Sander A. Mann: 0000-0002-7742-0615
Zhiyong Fan: 0000-0002-5397-0129
Shannon W. Boettcher: 0000-0001-8971-9123

DOI: 10.1021/acs.nanolett.7b02213
Nano Lett. 2017, 17, 6557−6563

Author Contributions

S.Z.O. and P.K. contributed equally to the work. E.C.G., S.Z.O., and P.K. conceived the experiment. S.Z.O. and P.K. performed the nanowire synthesis with assistance from S.B. S.Z.O. performed the TEM and diffraction measurements. P.K. performed the PL measurements with assistance from SAM. Q.Z. prepared the custom-made AAO templates. E.C.G., Z.F., and S.W.B. supervised the research. All authors contributed to the manuscript.

Notes

The authors declare no competing financial interest.

■ ACKNOWLEDGMENTS

We acknowledge Gede Adhyaksa for Al_2O_3 ALD, Joshua Razink for the TEM support, Beniamino Sciacca for discussions about AAO, Yuan Gao for assistance in preparing AAO templates, and Joseph Huber from InRedox for helpful discussions. The work at AMOLF is part of the research program of the "Nederlandse Organisatie voor Wetenschappelijk Onderzoek" (NWO). This work was supported by the NWO VIDI grant (project number 14846) and by the European Research Council (grant agreement no. 337328) and by an industrial partnership between Philips and AMOLF. The work at the University of Oregon was supported through a Cottrell Scholar Award by the Research Corporation for Science Advancement and the Sloan Research Fellowship by the Alfred P. Sloan Foundation. The work in The Hong Kong University of Science and Technology was supported by General Research Fund (project 16237816) from the Hong Kong Research Grant Council, and National Natural Science Foundation of China (project 51672231). Furthermore, we acknowledge the use of the CAMCOR shared instrument facility at the University of Oregon, which is supported by grants from the M. J. Murdock Charitable Trust, the W. M. Keck Foundation, ONAMI, and the NSF.

■ REFERENCES

(1) Brenner, T. M.; Egger, D. A.; Kronik, L.; Hodes, G.; Cahen, D. *Nat. Rev. Mater.* **2016**, *1* (1), 15007.
(2) Zhang, W.; Eperon, G. E.; Snaith, H. J. *Nat. Energy* **2016**, *1* (6), 16048.
(3) Mann, S. A.; Grote, R. R.; Osgood, R. M.; Alù, A.; Garnett, E. C. *ACS Nano* **2016**, *10* (9), 8620−8631.
(4) Brongersma, M. L.; Cui, Y.; Fan, S. *Nat. Mater.* **2014**, *13* (5), 451−460.
(5) Ferry, V. E.; Verschuuren, M. A.; Li, H. B. T.; Verhagen, E.; Walters, R. J.; Schropp, R. E. I.; Atwater, H. A.; Polman, A. *Opt. Express* **2010**, *18* (102), 237−245.
(6) Mann, S. A.; Garnett, E. C. *Nano Lett.* **2013**, *13* (7), 3173−3178.
(7) Garnett, E.; Yang, P. *Nano Lett.* **2010**, *10* (3), 1082−1087.
(8) Wallentin, J.; Anttu, N.; Asoli, D.; Huffman, M.; Aberg, I.; Magnusson, M. H.; Siefer, G.; Fuss-Kailuweit, P.; Dimroth, F.; Witzigmann, B.; Xu, H. Q.; Samuelson, L.; Deppert, K.; Borgstrom, M. T. *Science* **2013**, *339* (6123), 1057−1060.
(9) Polman, A.; Atwater, H. a. *Nat. Mater.* **2012**, *11* (3), 174−177.
(10) Yu, Z.; Raman, A.; Fan, S. *Proc. Natl. Acad. Sci. U. S. A.* **2010**, *107* (41), 17491−17496.
(11) Mann, S. A.; Garnett, E. C. *ACS Photonics* **2015**, *2* (7), 816−821.
(12) Deng, W.; Huang, L.; Xu, X.; Zhang, X.; Jin, X.; Lee, S.-T.; Jie, J. *Nano Lett.* **2017**, *17* (4), 2482−2489.
(13) Zhang, D.; Yu, Y.; Bekenstein, Y.; Wong, A. B.; Alivisatos, A. P.; Yang, P. *J. Am. Chem. Soc.* **2016**, *138* (40), 13155−13158.
(14) Daubinger, P.; Kieninger, J.; Unmüssig, T.; Urban, G. a. *Phys. Chem. Chem. Phys.* **2014**, *16* (18), 8392−8399.
(15) Petrov, A. A.; Pellet, N.; Seo, J.-Y.; Belich, N. A.; Kovalev, D. Y.; Shevelkov, A. V.; Goodilin, E. A.; Zakeeruddin, S. M.; Tarasov, A. B.; Graetzel, M. *Chem. Mater.* **2017**, *29* (2), 587−594.
(16) Park, K.; Lee, J. W.; Kim, J. D.; Han, N. S.; Jang, D. M.; Jeong, S.; Park, J.; Song, J. K. *J. Phys. Chem. Lett.* **2016**, *7* (18), 3703−3710.
(17) Eaton, S. W.; Lai, M.; Gibson, N. A.; Wong, A. B.; Dou, L.; Ma, J.; Wang, L.-W.; Leone, S. R.; Yang, P. *Proc. Natl. Acad. Sci. U. S. A.* **2016**, *113* (8), 1993−1998.
(18) Deng, H.; Dong, D.; Qiao, K.; Bu, L.; Li, B.; Yang, D.; Wang, H.-E.; Cheng, Y.; Zhao, Z.; Tang, J.; Song, H. *Nanoscale* **2015**, *7* (9), 4163−4170.
(19) Zhu, H.; Fu, Y.; Meng, F.; Wu, X.; Gong, Z.; Ding, Q.; Gustafsson, M. V.; Trinh, M. T.; Jin, S.; Zhu, X.-Y. *Nat. Mater.* **2015**, *14* (6), 636−642.
(20) Im, J.-H.; Luo, J.; Franckevičius, M.; Pellet, N.; Gao, P.; Moehl, T.; Zakeeruddin, S. M.; Nazeeruddin, M. K.; Grätzel, M.; Park, N.-G. *Nano Lett.* **2015**, *15* (3), 2120−2126.
(21) Richter, J. M.; Abdi-Jalebi, M.; Sadhanala, A.; Tabachnyk, M.; Rivett, J. P. H.; Pazos-Outón, L. M.; Gödel, K. C.; Price, M.; Deschler, F.; Friend, R. H. *Nat. Commun.* **2016**, *7*, 13941.
(22) Spina, M.; Bonvin, E.; Sienkiewicz, A.; Náfrádi, B.; Forró, L.; Horváth, E. *Sci. Rep.* **2016**, *6* (1), 19834.
(23) Xing, J.; Liu, X. F.; Zhang, Q.; Ha, S. T.; Yuan, Y. W.; Shen, C.; Sum, T. C.; Xiong, Q. *Nano Lett.* **2015**, *15* (7), 4571−4577.
(24) Wong, A. B.; Lai, M.; Eaton, S. W.; Yu, Y.; Lin, E.; Dou, L.; Fu, A.; Yang, P. *Nano Lett.* **2015**, *15* (8), 5519−5524.
(25) Ashley, M. J.; O'Brien, M. N.; Hedderick, K. R.; Mason, J. A.; Ross, M. B.; Mirkin, C. A. *J. Am. Chem. Soc.* **2016**, *138* (32), 10096−10099.
(26) Waleed, A.; Tavakoli, M. M.; Gu, L.; Wang, Z.; Zhang, D.; Manikandan, A.; Zhang, Q.; Zhang, R.-J.; Chueh, Y.-L.; Fan, Z. *Nano Lett.* **2017**, *17* (1), 523−530.
(27) Gu, L.; Tavakoli, M. M.; Zhang, D.; Zhang, Q.; Waleed, A.; Xiao, Y.; Tsui, K.-H.; Lin, Y.; Liao, L.; Wang, J.; Fan, Z. *Adv. Mater.* **2016**, *28* (44), 9713−9721.
(28) Tavakoli, M. M.; Waleed, A.; Gu, L.; Zhang, D.; Tavakoli, R.; Lei, B.; Su, W.; Fang, F.; Fan, Z. *Nanoscale* **2017**, *9* (18), 5828−5834.
(29) Lafalce, E.; Zhang, C.; Zhai, Y.; Sun, D.; Vardeny, Z. V. *J. Appl. Phys.* **2016**, *120* (14), 143101.
(30) Cho, H.; Jeong, S.-H.; Park, M.-H.; Kim, Y.-H.; Wolf, C.; Lee, C.-L.; Heo, J. H.; Sadhanala, A.; Myoung, N.; Yoo, S.; Im, S. H.; Friend, R. H.; Lee, T.-W. *Science* **2015**, *350* (6265), 1222−1225.
(31) Sutter-Fella, C. M.; Li, Y.; Amani, M.; Ager, J. W.; Toma, F. M.; Yablonovitch, E.; Sharp, I. D.; Javey, A. *Nano Lett.* **2016**, *16* (1), 800−806.
(32) Wen, L.; Xu, R.; Mi, Y.; Lei, Y. *Nat. Nanotechnol.* **2016**, *12* (3), 244−250.
(33) Elam, J. W.; Routkevitch, D.; Mardilovich, P. P.; George, S. M. *Chem. Mater.* **2003**, *15* (18), 3507−3517.
(34) Lee, W.; Park, S.-J. *Chem. Rev.* **2014**, *114* (15), 7487−7556.
(35) Masuda, H.; Abe, A.; Nakao, M.; Yokoo, A.; Tamamura, T.; Nishio, K. *Adv. Mater.* **2003**, *15* (2), 161−164.
(36) Yanagishita, T.; Sasaki, M.; Nishio, K.; Masuda, H. *Adv. Mater.* **2004**, *16* (5), 429−432.
(37) Smith, J. T.; Hang, Q.; Franklin, A. D.; Janes, D. B.; Sands, T. D. *Appl. Phys. Lett.* **2008**, *93* (4), 043108.
(38) Robatjazi, H.; Bahauddin, S. M.; Macfarlan, L. H.; Fu, S.; Thomann, I. *Chem. Mater.* **2016**, *28* (13), 4546−4553.
(39) Tian, M.; Xu, S.; Wang, J.; Kumar, N.; Wertz, E.; Li, Q.; Campbell, P. M.; Chan, M. H. W.; Mallouk, T. E. *Nano Lett.* **2005**, *5* (4), 697−703.
(40) Guo, Y.; Shoyama, K.; Sato, W.; Matsuo, Y.; Inoue, K.; Harano, K.; Liu, C.; Tanaka, H.; Nakamura, E. *J. Am. Chem. Soc.* **2015**, *137* (50), 15907−15914.
(41) Jeon, N. J.; Noh, J. H.; Kim, Y. C.; Yang, W. S.; Ryu, S.; Seok, S. Il. *Nat. Mater.* **2014**, *13* (9), 897−903.
(42) Williams, S. T.; Chueh, C.-C.; Jen, A. K.-Y. *Small* **2015**, *11* (26), 3088−3096.

DOI: 10.1021/acs.nanolett.7b02213
Nano Lett. 2017, 17, 6557−6563

(43) Jeong, B.; Hwang, I.; Cho, S. H.; Kim, E. H.; Cha, S.; Lee, J.; Kang, H. S.; Cho, S. M.; Choi, H.; Park, C. *ACS Nano* **2016**, *10* (9), 9026−9035.
(44) Ko, M.; Baek, S. H.; Song, B.; Kang, J. W.; Kim, S. A.; Cho, C. H. *Adv. Mater.* **2016**, *28* (13), 2504−2510.
(45) Cao, L.; White, J. S.; Park, J.-S.; Schuller, J. A.; Clemens, B. M.; Brongersma, M. L. *Nat. Mater.* **2009**, *8* (8), 643−647.
(46) Noh, J. H.; Im, S. H.; Heo, J. H.; Mandal, T. N.; Seok, S. Il. *Nano Lett.* **2013**, *13* (4), 1764−1769.
(47) Yan, J.; Ke, X.; Chen, Y.; Zhang, A.; Zhang, B. *Appl. Surf. Sci.* **2015**, *351*, 1191−1196.
(48) Woodward, D. I.; Reaney, I. M. *Acta Crystallogr., Sect. B: Struct. Sci.* **2005**, *61* (4), 387−399.
(49) Yu, Y.; Zhang, D.; Kisielowski, C.; Dou, L.; Kornienko, N.; Bekenstein, Y.; Wong, A. B.; Alivisatos, A. P.; Yang, P. *Nano Lett.* **2016**, *16* (12), 7530−7535.
(50) Klein-Kedem, N.; Cahen, D.; Hodes, G. *Acc. Chem. Res.* **2016**, *49* (2), 347−354.
(51) Yan, J.; Zhang, B.; Chen, Y.; Zhang, A.; Ke, X. *ACS Appl. Mater. Interfaces* **2016**, *8* (20), 12756−12763.
(52) Mann, S. A.; Sciacca, B.; Zhang, Y.; Wang, J.; Kontoleta, E.; Liu, H.; Garnett, E. C. *ACS Nano* **2017**, *11* (2), 1412−1418.
(53) Mann, S. A.; Oener, S. Z.; Cavalli, A.; Haverkort, J. E. M.; Bakkers, E. P. A. M.; Garnett, E. C. *Nat. Nanotechnol.* **2016**, *11* (12), 1071−1075.
(54) Luo, Y.; Khoram, P.; Brittman, S.; Zhu, Z.; Lai, B.; Ong, S. P.; Garnett, E. C.; Fenning, D. P. *Adv. Mater.* **2017**, 1703451.
(55) Matteocci, F.; Cinà, L.; Lamanna, E.; Cacovich, S.; Divitini, G.; Midgley, P. A.; Ducati, C.; Di Carlo, A. *Nano Energy* **2016**, *30* (July), 162−172.
(56) Weerasinghe, H. C.; Dkhissi, Y.; Scully, A. D.; Caruso, R. A.; Cheng, Y. B. *Nano Energy* **2015**, *18*, 118−125.
(57) Raja, S. N.; Bekenstein, Y.; Koc, M. A.; Fischer, S.; Zhang, D.; Lin, L.; Ritchie, R. O.; Yang, P.; Alivisatos, A. P. *ACS Appl. Mater. Interfaces* **2016**, *8* (51), 35523−35533.
(58) Tsai, H.; Nie, W.; Lin, Y.-H.; Blancon, J. C.; Tretiak, S.; Even, J.; Gupta, G.; Ajayan, P. M.; Mohite, A. D. *Adv. Energy Mater.* **2017**, *7*, 1602159.
(59) Namkoong, G.; Mamun, A. A.; Ava, T. T.; Zhang, K.; Baumgart, H. *Org. Electron.* **2017**, *42*, 228−233.
(60) Cohen, B. El; Etgar, L. *Front. Optoelectron.* **2016**, *9* (1), 44−52.
(61) Huang, J.; Yu, X.; Xie, J.; Xu, D.; Tang, Z.; Cui, C.; Yang, D. *ACS Appl. Mater. Interfaces* **2016**, *8* (33), 21505−21511.
(62) Eperon, G. E.; Habisreutinger, S. N.; Leijtens, T.; Bruijnaers, B. J.; Van Franeker, J. J.; Dequilettes, D. W.; Pathak, S.; Sutton, R. J.; Grancini, G.; Ginger, D. S.; Janssen, R. A. J.; Petrozza, A.; Snaith, H. J. *ACS Nano* **2015**, *9* (9), 9380−9393.
(63) Brittman, S.; Garnett, E. C. *J. Phys. Chem. C* **2016**, *120* (1), 616−620.

DOI: 10.1021/acs.nanolett.7b02213
Nano Lett. 2017, 17, 6557−6563